ACS APPLIED MATERIALS & INTERFACES

RESEARCH ARTICLE

www.acsami.org

The Effective Young's Modulus of Carbon Nanotubes in Composites

Libo Deng,[†] Stephen J. Eichhorn,[‡] Chih-Chuan Kao,[†] and Robert J. Young*[,†,‡]

[†]Materials Science Centre, School of Materials, Grosvenor Street, University of Manchester, Manchester, M13 9PL, U.K.

[‡]School of Materials and the Northwest Composites Centre, Paper Science Building, Sackville Street, University of Manchester, Manchester, M13 9PL, U.K.

Supporting Information

ABSTRACT: A detailed study has been undertaken of the efficiency of reinforcement in nanocomposites consisting of single-walled carbon nanotubes (SWNTs) in poly(vinyl alcohol) (PVA). Nanocomposite fibers have been prepared by electrospinning and their behavior has been compared with nanocomposite films of the same composition. Stress transfer from the polymer matrix to the nanotubes has been followed from stress-induced Raman band shifts, which are shown to be controlled by both geometric factors such as the angles between the nanotube axis, the stressing direction and the direction of laser polarization, and by finite length effects and bundling. A theory has been developed that takes into account all of these factors and enables the behavior of the different forms of nanocomposite, both fibers and films, to be compared in different polarization configurations. The effective modulus of the SWNTs has been found to be in the range 530−700 GPa which, while being impressive, is lower than the generally accepted value of around 1000 GPa as a result of factors such as finite length effects and nanotube bundling. This value of effective modulus has, however, been shown to be consistent with the contribution of nanotubes to the 20% increase in Young's modulus found for the nanocomposite films with a loading of only 0.2% of SWNTs. Hence a self-consistent method has been developed which enables the efficiency of reinforcement by nanotubes, and potentially other high-aspect-ratio nanoparticles, to be evaluated from stress-induced Raman bands shifts in nanocomposites independent of the specimen geometry and laser polarization configuration.

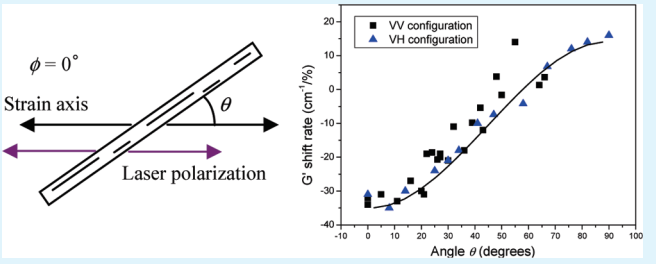

KEYWORDS: Raman spectroscopy, strain, SWNTs, nanocomposites, stress, Young's modulus

INTRODUCTION

Carbon nanotubes are known[1−4] to have high stiffness and strength. One of the best ways to exploit these properties is by incorporating them into polymer nanocomposites.[5] Well-defined Raman spectra can be obtained from carbon nanotubes and large shifts of the Raman bands occur when the nanotubes are subjected to stress.[6−8] This phenomenon can be used to follow the deformation of carbon nanotubes within a polymer matrix and can be employed as an indication of stress transfer from the matrix to the nanotubes.[9] In general, the highest Raman band shift per unit strain is observed when all nanotubes are oriented along both the directions of maximum strain and concurrently of laser polarization.[10,11]

In many situations the alignment of the nanotubes in one direction in a nanocomposite is required to maximize their properties as mechanical reinforcing fillers.[12] Although a variety of methods such as melt-spinning, magnetic fields,[13] and gel spinning[14] have been employed to achieve good nanotube orientation, electrospinning has proved to be a particularly effective technique to disperse and align nanotubes in polymer matrix.[15] Several groups have observed a virtually perfect orientation for nanotubes in electrospun fibers, and reinforcement due to the presence of aligned nanotubes has been observed.[16,17] Our group has recently demonstrated high efficiency of stress transfer to SWNTs in an individual electrospun PVA fiber through the observation of the large stress-induced shifts of the G′ Raman band during deformation.[18,19]

In this present study, we have prepared both PVA/SWNT nanocomposite fibers containing highly aligned nanotubes and PVA/SWNT nanocomposite isotropic films containing unoriented nanotubes using electrospinning and a solution-casting method, respectively. The effect of orientation and crystallinity of polymers upon stress transfer during deformation has been investigated using Raman spectroscopy. We demonstrate that the shift rate with strain of the nanotube G′ Raman band is dependent on the angles between the nanotube axis, strain direction and the direction of laser polarization; the angular-dependent Raman response also depends upon the polarization configuration of the Raman spectrometer. We explain this behavior using a model that takes into account the contribution of nanotubes aligned in different directions in the composites, the resolved stress on the

Received: October 20, 2010
Accepted: December 13, 2010
Published: January 10, 2011

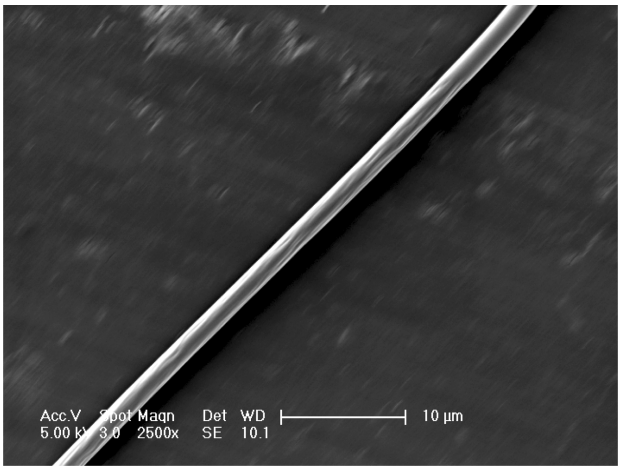

Figure 1. SEM micrograph of a single electrospun nancomposite fiber.

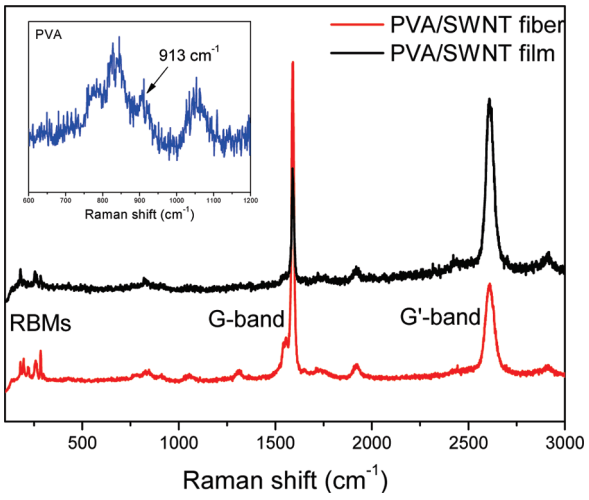

Figure 2. Raman spectra obtained from a single electrospun PVA/SWNT fiber and a PVA/SWNT film. (The spectra have been offset for clarity and the region of the spectrum showing the PVA bands is inset.)

nanotubes, the Poisson's contraction and the polarization configuration. Moreover, the model can also be used to explain the efficiency of mechanical reinforcement in the PVA/SWNT nanocomposite film. Our approach has major implications on the interpretation of nanocomposite properties and shows that the contribution of the effective modulus in a randomly oriented SWNT composite is consistent with bulk mechanical properties. This also has general implications for nanocomposites utilizing a wider range of reinforcing fillers with high aspect ratios, other than SWNTs.

RESULTS AND DISCUSSION

Morphology of the Electrospun Fibers. Narrow-diameter electrospun nanocomposite fibers, an example of which is shown in Figure 1, were collected after being aligned macroscopically using the rotating disk. The fiber diameter was controlled by varying the processing conditions such as the concentration of polymer solution, the flow rate, and the speed of disk rotation. The average diameter decreased from 700 nm for fibers collected at 0 rpm (a grounded stationary stage) to 590 nm for those

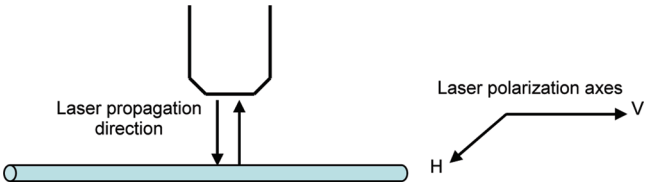

Figure 3. Schematic diagram of the configuration of the laser polarization.

collected with a disk rotating at an angular velocity of 1500 rpm. The macroscopic orientation of the fibers collected on the PMMA beam could be controlled by changing the position of the beam on the rotating disk relative to the direction of disk rotation.

Raman Characterization. Figure 2 shows the Raman spectra of a single PVA/SWNT fiber and the PVA/SWNT composite film. Because of the resonantly enhanced signal from the nanotubes[20], well-defined Raman bands such as the radial breathing modes (RBMs), G-band and G′-band from nanotubes can be seen even at the low loadings of nanotubes employed (0.2%). It should be noted that the G′-band position in the electrospun fibers collected at 0 rpm is 2 cm^{-1} higher than in the film while the G′-band position in fibers collected with 1500 rpm is 2 cm^{-1} lower than in the films. This suggests that the electrospinning process alone induces a small residual compression of the nanotubes in the fibers, possibly due to shrinkage as the solvent evaporates. In contrast, in fibers collected with a high-speed rotating disk, the nanotubes are prestretched and have a slight residual tension that is not relaxed by solvent evaporation. Weak but resolvable Raman bands in the 600−1200 cm^{-1} region corresponding to PVA polymer are shown in the inset. This also enables the orientation of the polymer to be followed through the use of Raman spectroscopy (see the Supporting Information, Figure S1).

The orientation of the nanotubes can be characterized using polarized Raman spectroscopy. This is based on the orientation-dependent Raman band intensity of nanotubes: the Raman band intensity is a maximum when the nanotube axis is parallel to both the incident and scatter laser and is a minimum when the nanotube is perpendicular to the laser polarization[21]. The configuration of laser polarization is denoted by a pair of letters such as "VV", "VH", "HH", and "HV", in which the first and second letters denote the polarization direction of the incident and scattered lasers, respectively. "V" and "H" indicate the lasers are parallel and perpendicular to the frame reference axis, respectively (Figure 3).

Figure 4a shows the intensity of the nanotube G-band of a single nanocomposite fiber oriented at different angles φ between the fiber axis and polarization of incident laser (the Raman intensities were normalized to the intensity at $\varphi = 0°$). It can be seen that the intensity decreases dramatically as the angle φ increases, indicating a high degree of alignment of the nanotubes in the fiber. The solid line is generated for an $I \propto \cos^4 \varphi$ function, which is expected to apply for perfect orientation of the nanotubes in the fiber[22]. The data follow the curve very closely until $\varphi > 60°$ but deviate a little from the theoretical line above this angle, showing some slight misorientation. The actual nanotube orientation factor is determined to be 0.92 using the method of Liu et al.[23,24]. The strong drawing force exerted by electrical field results in a high draw ratio in electrospinning jets and consequently a high degree of nanotube alignment.

Orientation of the nanotubes in the PVA/SWNT film was also investigated as shown in Figures 4b. It can be seen that the

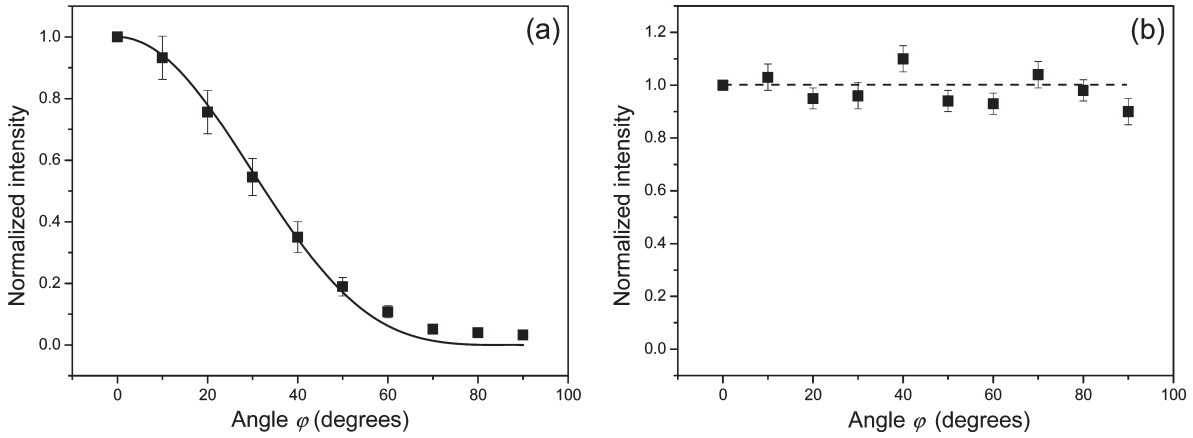

Figure 4. (a) Variation of nanotube G-band intensity as a function of the angle φ between the fiber axis and the polarization of incident laser for an electrospun PVA/SWNT fiber. (b) G-band intensity obtained for the PVA/SWNT film rotated at different angles φ. The dashed line is a guide to eyes.

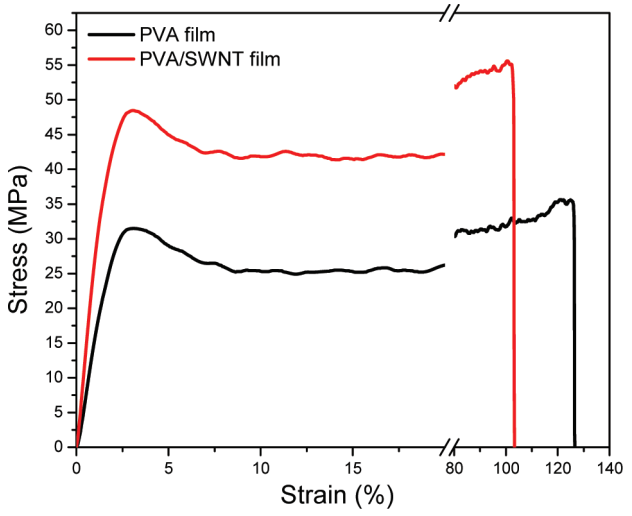

Figure 5. Typical stress−strain curves of neat PVA and PVA/SWNT nanocomposite films.

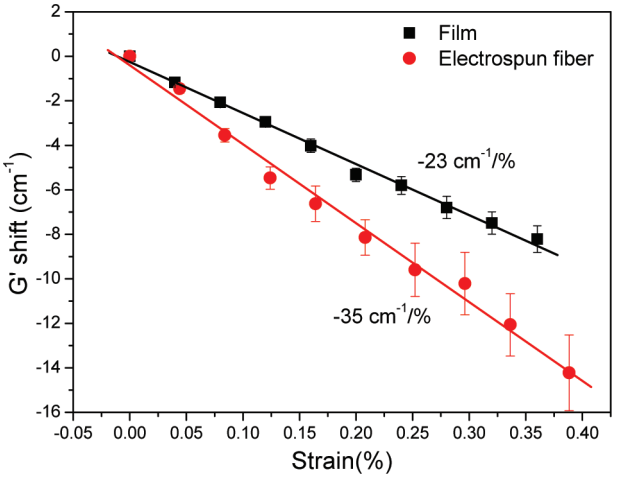

Figure 6. Variation of the position of the G′-band for nanotubes in a PVA/SWNT fiber and film as a function of strain.

intensity of nanotube G-band does not change significantly when measured at different angles within the plane of the film relative to an arbitrarily chosen axis. This suggests that the nanotubes are uniformly distributed in all directions in this nanocomposite film.

Mechanical Properties of the PVA/SWNT Nanocomposite Film. Mechanical properties of the neat PVA and PVA/SWNT films were tested using an Instron testing machine and typical stress−strain curves are shown in Figure 5. It was found that the modulus increased from 1.9 ± 0.2 GPa for neat PVA to 2.3 ± 0.3 GPa for the PVA/SWNT composite film (a 20% improvement) and the tensile strength increased from 36 ± 5 MPa to 42 ± 6 MPa (a 15% improvement) with just 0.2% of SWNTs in the composite film. This mechanical reinforcement is found to originate from stress transfer to the nanotubes and is not due to any crystallization of the PVA induced by the presence of the nanotubes (see Figure S2 in the Supporting Information for the characterization of the crystallinity of the PVA using Raman spectroscopy).

Stress-Induced Raman Band Shifts. PVA/SWNT electrospun fibers and PVA/SWNT films prepared from the same solution were deposited on PMMA beams and deformed using a four-point bending rig. Figure 6 shows the stress-induced shift of the G′-band for both a fiber and film, where the Raman spectra were acquired with the VV configuration and the strain axis parallel to the laser polarization. The shift of G′-band to lower wavenumber is understood on the basis of the elongation of carbon−carbon bonds and decrease of force constants under tensile strain[25]. The nanotube G′-band shift per unit strain (i.e., the G′-band shift rate), observed in the elastic deformation region in PVA/SWNT films, of −23 cm^{-1}/% strain, is to the best of our knowledge one of the highest found in isotropic polymer/nanotube films and is higher than in many nanotube composite fibers.[26] The high shift rates found in these composites is attributed to good stress transfer from the PVA matrix to the nanotubes due to the good dispersion of nanotubes in the film. It appears that the PVA polymer facilitates and stabilizes the dispersion of nanotubes in the nanocomposites as found before.[14] A controlled experiment was undertaken to assess the effect of dispersion upon the Raman band shift rate. The PVA/SWNT suspension was dispersed with shorter sonication times and the resultant film, with a poorer dispersion of nanotubes exhibited a significantly lower band-shift rate (see the Supporting Information, Figure S3). The electrospun fiber in Figure 6 exhibited an even higher Raman band shift rate of −35 cm^{-1}/% strain, which will be shown to be a consequence of the better orientation of both the nanotubes and polymer molecules compared to the film.

dx.doi.org/10.1021/am1010145 |ACS Appl. Mater. Interfaces 2011, 3, 433–440

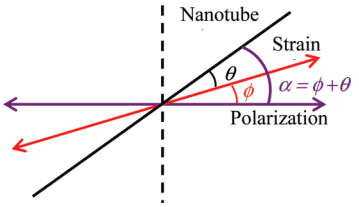

Figure 7. Schematic diagram of the angles between the nanotube axis, strain axis, and the laser polarization direction in the same plane.

Angular Dependence of the Deformation Behavior. The stress-induced Raman band shift rate for nanotubes has been found to be dependent on the polarization configuration and the angle between the nanotube axis and the strain direction[10,11]. An understanding of the influence of these factors is required if the Raman band shift rate is to be used to assess the mechanical reinforcement efficiency of nanotubes in composites. A detailed study was thus undertaken to assess the level of stress-induced Raman band shift for the PVA/SWNT nanocomposite fibers and films as function of the angles between the direction of incident laser polarization and the nanotube axis (α) and strain axis (ϕ). The definitions of these angles are shown in Figure 7 where the angle θ is defined as the angle between the strain axis and nanotube axis ($\alpha = \phi + \theta$). The nanotubes are assumed to be aligned perfectly along the length of the electrospun fibers and distributed uniformly in all directions in the plane of the films.

The shift of the G′-band was measured as a function of strain for the nanotubes in the PVA/SWNT fibres and films in three different experimental arrangements shown in Figure 8. The slope of the lines, similar to those plotted in Figure 6, gives the G′-band shift rate. The G′-band shift rate was determined as a function of angle for three different geometries investigated.

1. Nanocomposite Fiber (θ = 0° and ϕ varied). An electrospun fiber adhering to a PMMA beam was deformed axially ($\theta = 0°$) using the four-point bending rig. Since the strain direction is parallel to the fiber axis then $\phi \equiv \varphi$. This angle was changed relative to the direction of incident laser polarization by rotating the rig on the Raman microscope stage and the G′-band shift rate with strain was recorded as a function of ϕ. Measurements were undertaken using two different polarization configurations, VV and VH. When the VV configuration was used, it was difficult to go beyond 60° as the Raman signal became weak at higher angles because of the $\cos^4\phi$ dependence of the intensity (Figure 4a). It can be seen from Figure 8a, however, that the shift rates are constant with angle, suggesting that the nanotubes are always subject to the same stress in this geometry, so that the band shift is independent of the polarization configuration. The band shift rate found using the VH configuration revealed that the shift rate was also independent of the polarization of the scattered light in this case.

2. Nanocomposite Fiber (ϕ = 0° and θ varied). Stress was applied to single electrospun fibers lying at different angles on the beam and the G′-band shift rate determined as a function of θ, the angle between nanotube ($\equiv$ fiber) axis and strain axis as shown in Figure 8b. The down-shift rate of the Raman band becomes smaller as θ increases and the G′-band shift rate is observed to become positive when the angle exceeds 55°, suggesting that the nanotubes become subjected to compression at higher angles because of the compression of the PVA matrix, which is associated with the Poisson's contraction effect.

As the nanotubes are parallel to the fiber axis, the axial strain in nanotubes is assumed to be identical to the strain in the fiber, and the Raman band shift then scales with the strain in the fiber. Andrews et al.[27]. have shown that the Raman band shift rate for a Kevlar fiber in a composite lying at an angle θ with respect to the strain axis, $S(\theta)$, is given by

$$S(\theta) = S_0(\cos^2\theta - \nu\sin^2\theta) \quad (1)$$

where ν is the Poisson's ratio of the matrix and S_0 is the band shift rate determined for the fiber parallel to the strain direction. Equation 1 can also be used to explain the angular dependence of the nanotube G′-band shift rate in the PVA nanocomposite fibers. The parameter S_0 is the G′-band shift rate when all nanotubes are aligned parallel to both the strain direction (i.e., $\theta = 0°$) and the laser polarization in this case, which can be seen to be -35 cm^{-1}/% (i.e., the electrospun fibers) in Figure 5 and is independent of the polarization configuration as shown in Figure 8a. The values of Poisson's ratio for polymers are typically between 0.33 and 0.49 and are not known accurately for all polymers[28]. The curve in Figure 8b is generated from eq 1 assuming a Poisson's ratio of 0.4 for both the PMMA beam and PVA and it can be seen from Figure 8b that the data fall close to the curve. This confirms the validity of eq 1 for the deformation of the electrospun fibers. The shift rate was again found to be independent of the polarization configuration, i.e., the shift rate detected with the VH configuration is similar to the VV configuration.

3. Nanocomposite Film (ϕ varied). The nanocomposite film was deformed at different angles ϕ with respect to the direction of laser polarization (Figure 8c) and the G′-band shift monitored as a function of strain for two different polarization configurations, VV and VH. Since the nanotubes are oriented randomly in the plane of the film, the Raman band has contributions from nanotubes lying in all directions in the film. When the VV configuration is used, the negative shift rate decreases as the angle ϕ increases and the shift rate becomes positive above 75°, again due to the Poisson's contraction effect.

Nanotubes contribute to the Raman band intensity differently when the VH configuration is used rather than in the VV configuration. Because of this, a constant angular-dependent shift rate was observed for VH as can be seen from Figure 8c. These phenomena can be analyzed quantitatively if both the resolved stress on the nanotubes and the orientation dependence of Raman intensity of the nanotubes are taken into account.

The Raman intensity for the PVA/SWNT film is due to a contribution of nanotubes lying in all directions. Assuming the nanotubes are uniformly distributed in all directions, the proportion of nanotubes lying within an infinitesimal angle range dα with respect to the polarization direction is $1/\pi$dα. The Raman intensity, I, for VV and VH configurations is given by[21,22]

$$I_{VV}(\alpha) = \frac{1}{\pi}\int_0^{\pi} I_0\cos^4\alpha\,d\alpha \quad (2)$$

$$I_{VH}(\alpha) = \frac{1}{\pi}\int_0^{\pi} I_0'\cos^2\alpha\sin^2\alpha\,d\alpha \quad (3)$$

At a given angle ϕ the intensities can then be described by

$$I_{VV}(\phi) = \frac{1}{\pi}\int_0^{\pi} I_0\cos^4(\theta+\phi)d\theta \quad (4)$$

$$I_{VH}(\phi) = \frac{1}{\pi}\int_0^{\pi} I_0'\cos^2(\theta+\phi)\sin^2(\theta+\phi)d\theta \quad (5)$$

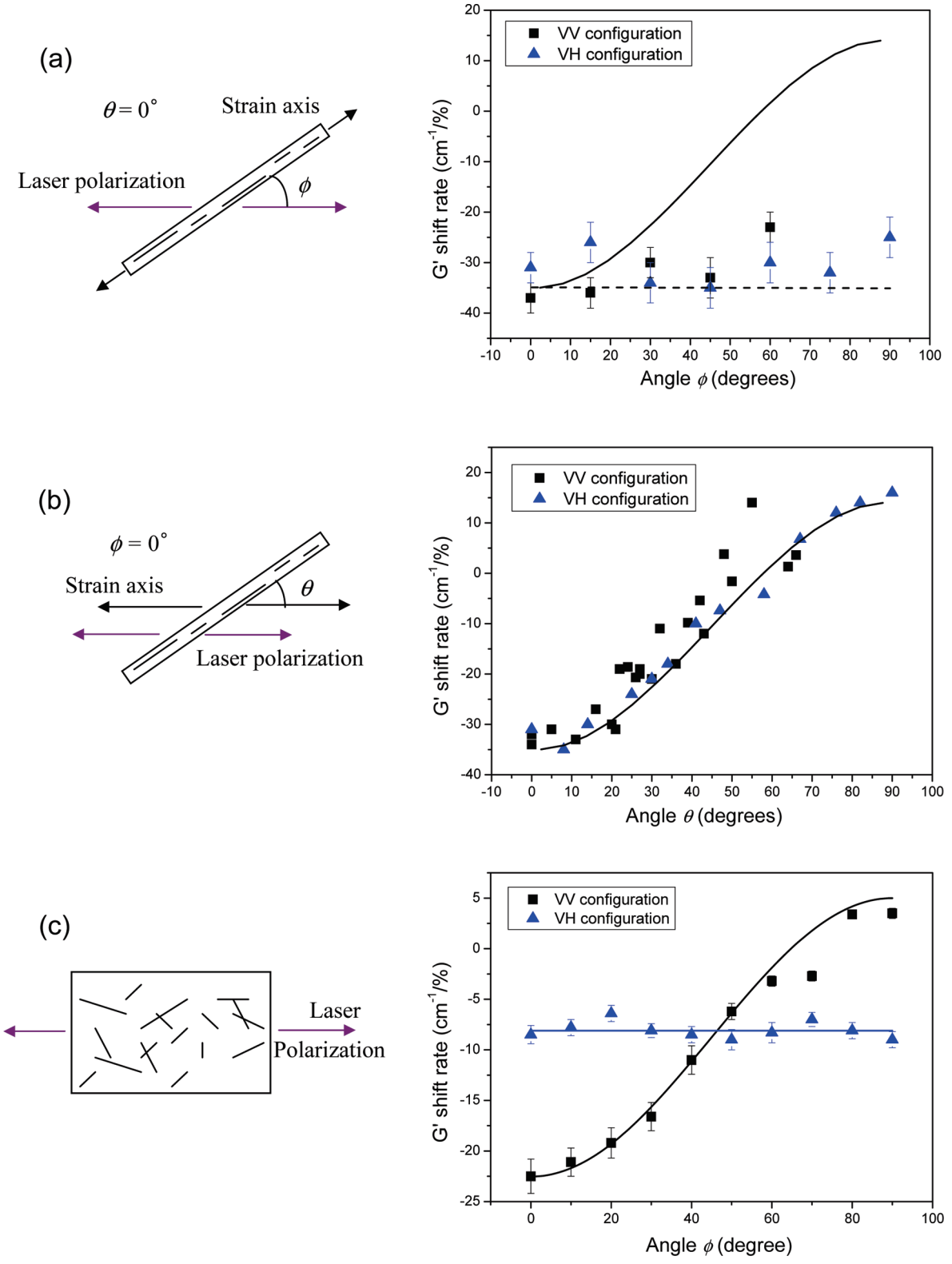

Figure 8. Nanotube G′-band shift rate as a function of the angles between (a) the strain axis and laser polarization for an electrospun fiber, (b) the strain axis and nanotube axis for an electrospun fiber, and (c) the strain axis and laser polarization axis for the isotropic film. The lines in a and b are generated using eq 1 with $S_0 = -35$ cm^{-1}/% strain, and the lines in c are generated using eqs 6 and 7 with $S_0 = -29.5$ cm^{-1}/% strain and -27 cm^{-1}/% for VV and VH configurations, respectively.

where I_0 and I'_0 are parameters that give the maximum intensity for each configuration. The stress-induced Raman band shift for the film can be considered as an intensity-weighted average of the contributions of all the individual nanotubes aligned at different

Table 1. Calculated Effective Modulus of Nanotubes and the Composite Modulus Based on the G′-Band Shift Rate Detected at $\phi = 0°$ (i.e., laser polarization parallel to the strain direction)

material	polarization	shift rate, S_0 (cm^{-1}/%)	nanotube effective modulus, E_{eff} (GPa)	predicted composite modulus, E_c (GPa)
PVA/SWNT fiber	VV	−35	700	
PVA/SWNT film	VV	−23	600	2.4 ± 0.2
PVA/SWNT film	VH	−8	530	2.3 ± 0.2

angles in the nanocomposite[10]. The contribution of each nanotube to the shift of the G′-band can be described by the Raman intensity multiplied by its band shift. For nanotubes distributed uniformly in two-dimensions in the film, the dependencies of the shift rates for the two different polarization configurations, VV and VH, upon the angle ϕ are then given by

$$S_{VV}(\phi) = \frac{\frac{1}{\pi}\int_0^{\pi} I_0\cos^4(\theta+\phi) \times [S_0(\cos^2\theta - \nu\sin^2\theta)]d\theta}{\frac{1}{\pi}\int_0^{\pi} I_0\cos^4(\theta+\phi)d\theta} \quad (6)$$

$$S_{VH}(\phi) = \frac{\frac{1}{\pi}\int_0^{\pi} I_0'[\cos^2(\theta+\phi)\sin^2(\theta+\phi)] \times [S_0(\cos^2\theta - \nu\sin^2\theta)]d\theta}{\frac{1}{\pi}\int_0^{\pi} I_0'[\cos^2(\theta+\phi)\sin^2(\theta+\phi)]d\theta} \quad (7)$$

where the Poisson's ratio ν can be taken as 0.40 for both the PVA and PMMA. Frogley et al. also considered the intensity-weighted average of the contributions of individual nanotubes to the overall band shift.[10] The validity of the theory is verified here by measuring the G′-band shift rate at different angles.

A least-squares fit of eqs 6 and 7 to the experimental data in Figure 8c gives $S_0 = -29.5$ cm^{-1}/% for the VV configuration and -27 cm^{-1}/% for the VH configuration, suggesting good consistency for S_0 values determined with different configurations. The slightly different values are due to the variation between the specimens and S_0 is seen to be independent of the polarization configuration. It is noted that these values, which represent the G′-band shift rate when the nanotubes are parallel to the strain axis in PVA films, are lower than the shift rate observed in the electrospun fiber (-35 cm^{-1}/%). This is probably due to the improved orientation and crystallinity of PVA polymer in the electrospun fiber, which resulted in a stronger interface and consequently led to better efficiency of stress transfer in the electrospun fiber than in the film.

Extension of the theory to three dimensions shows that the Raman band shift rate will be independent of the angle ϕ if nanotubes are distributed uniformly in three-dimensions in the film (see the Supporting Information). The agreement between theory and experiment in Figure 8c indicates that the nanotubes are distributed preferentially in two-dimensions in the plane of the nanocomposite film. The theory is only strictly valid at low strains because the nanotubes will tend to be become aligned as the strain is increased; our Raman data are all for strains of <0.5%.

Prediction of Composite Mechanical Properties. It is now possible to estimate the mechanical properties such as the modulus E_c of the composite film using the simple rule of mixtures[29] for nanotube-reinforced composites

$$E_c = \eta_o V_{NT} E_{eff} + (1 - V_{NT})E_m \quad (8)$$

where E_{eff} is the effective modulus of nanotube, E_m is the matrix modulus, V_{NT} is the volume fraction of nanotubes and η_o is a factor that takes into account the effect of the orientation of the nanotubes which is unity for a perfectly aligned system and is found to be 3/8 for 2D random system[9]. It is known that nanotube bundling[30,31] and finite length effects[29,32] will reduce the effective modulus below the nanotube Young's modulus E_{NT} such that:

$$E_{eff} = \eta_l E_{NT} \quad (9)$$

where the parameter η_l accounts for the reduction in effective nanotube modulus due to the nanotubes both having finite length and being bundled. The value of η_l will be reduced if the nanotubes become shorter through damage and will clearly increase as the dispersion is improved (see Supporting Information, Figure S3). This parameter is therefore useful in being able to gage the efficiency of reinforcement in the absence of orientation effects.

Cooper et al.[9] established a method to calculate the nanotube effective modulus using the stress-induced G′-band shift rate. They showed that the shift rate of G′-band of a number of different carbon fibers was proportional to the fiber modulus and went on to suggest that there was a universal calibration of -5 cm^{-1}%$^{-1}$/GPa for the stress-induced shifts of the G′-band in carbon fibers. Assuming that the calibration was also valid for the stress-induced shift of the same G′-band in carbon nanotubes, they used it to determine the effective Young's modulus of both single- and multiwalled carbon nanotubes in epoxy-matrix composites. The approach they used led to wide bounds in their estimation of modulus because they analyzed the cases of both random two- and three-dimensional nanotube arrangements but did not take into account laser polarization effects in their analysis. In this present study, we have been able to compare and model the behavior of both well-aligned nanocomposite fibers and a 2D random nanocomposite films and undertake measurements in different polarization configurations.

The effective modulus E_{eff} of the nanotubes in nanocomposites can be calculated if the shift rate S_0 is known since the universal calibration leads to[9]

$$E_{eff} = \frac{S_0}{-0.05} \quad (10)$$

where E_{eff} is in GPa and S_0 has units of cm^{-1}/% strain. For the unidirectionally aligned system (e.g., the electrospun fibers) it has been shown in Figure 8a that

$$S_0 = S(0) \quad (11)$$

where $S(0)$ is the shift rate obtained when the fiber is deformed parallel to the strain direction. For the randomly distributed system, S_0 can be estimated by fitting the shift rates obtained at different angles from eqs 6 and 7, or by simply by substituting

$\phi = 0°$ into eqs 6 and 7, which gives

$$S_0 = 1.3 \times S_{VV}(0) \quad (12)$$

$$S_0 = 3.3 \times S_{VH}(0) \quad (13)$$

These equations suggest that the effective moduli of nanotubes for composites containing randomly distributed nanotubes can be calculated by directly using the universal calibration (eq 10) and corrected by multiplying by a factor of 1.3 for those detected with the VV configuration or 3.3 for the VH configuration. These correction factors are significantly lower than those determined by Cooper et al.[9], where a value between 3 and 9 was suggested. Table 1 shows the values of E_{eff} determined using the different band shift rates, S_0 along with eqs 10− 13 where appropriate. It can be seen that the effective modulus of the nanotubes E_{eff} in the composites is in the range 530−700 GPa, i.e., about 50−70% of the accepted value of around 1000 GPa for nanotube modulus.[1−4]

Finally, it will be demonstrated how this analysis along with the 3/8 orientation factor for the films can be used to predict the Young's modulus of the nanocomposite. The volume fraction V_{NT} of nanotubes will be roughly the same as the weight fraction, i.e., 0.2%, because the SWNTs and PVA have about the same density ~1.3 g/cm^3. If E_{eff} is taken as 600 GPa (i.e., for E_{eff} determined with the VV configuration) and E_m is taken as 1.9 ± 0.2 GPa, substituting these values into eq 8 gives a 2.4 ± 0.2 GPa for E_c, which agrees well with the experimental result in Figure 5. The E_c evaluated using the E_{eff} determined for the VH configuration (Table 1) is also in good agreement with the experimental value. This demonstrates that this is a self-consistent method to evaluate the reinforcing efficiency of randomly distributed nanotubes.

CONCLUSIONS

Nanocomposite fibers in which nanotubes are highly aligned along fiber axis have been fabricated through the use of electrospinning equipped with a rotating disk. Very high Raman band shift rates per unit strain have been observed during deformation from the nanotubes in the nanocomposite fibers and films of the same composition. These shift rates have been found to depend strongly on the angles between the nanotube axis, strain direction and axis of laser polarization. A theory concerning the relationship between Raman band shift rate, the testing geometry and the effective modulus of nanotubes in composites has also been developed that takes into account all of these variables. It has been shown that the nanotubes in the system studied, consisting of PVA containing 0.2% by weight of nanotubes, have an effective Young's modulus that is around 50−70% of their theoretical value. This was shown to be entirely consistent with the level of reinforcement measured directly for films of the nanocomposite. The approach outlined in this study will enable the level of reinforcement to be assessed and refined in the future as a function of nanotube loading and processing conditions for similar nanocomposite systems, without having to prepare bulk nanocomposite samples.

EXPERIMENTAL SECTION

Materials and Sample Preparation. To prepare PVA/SWNT nanocomposite fibers and films, a solution consisting of 14% by weight of PVA polymer (molecular weight 85 000−124 000 g mol^{-1}, supplied by Sigma-Aldrich) and 0.2% by weight (relative to the polymer) of HiPco SWNTs was mixed and stirred in deionized water for 3 h. The suspension was then ultrasonicated using a sonic probe (Cole-Parmer Ultrasonic processor CPX 750) using a total sonication time of 30 min. Electrospinning was carried out with this solution immediately after the sonication. The spinning conditions were: voltage, 20 kV; flow rate, 0.01 mL/min; and needle tip-to-collector distance, 8 cm. The fibers were collected using either (1) a grounded stationary stage or (2) for deformation studies a rotating disk on which a PMMA beam was attached. The angular velocity of the disk was 1500 rpm.

The PVA/SWNT composite film was prepared by casting the sonicated solution onto a PMMA beam which was then left for 12 h to dry. Both the nanocomposite fibers and films were found to adhere well to the PMMA beams after drying.

Characterization. The morphology of the electrospun fibers was investigated after gold coating using a Philips XL30 FEG SEM, operated at an accelerating voltage of 5 kV. Raman spectra were obtained using a Renishaw 2000 system with a He−Ne laser. The laser spot size was about 2 μm, and the laser power was in the range 1−10 mW when the laser was focused onto the sample. A polarizer and $\lambda/2$ plates were inserted prior to the microscope entrance and/or after the notch filter to select the polarization directions for incident and scattered light. Four different polarization arrangements were employed: VV, polarization of both the incident laser beam and scattered light parallel to the principal axis of the spectrometer; VH, polarization of the incident laser beam parallel to the principal axis of the spectrometer and the polarization of the scattered light rotated by 90°; HH, polarization of both the incident laser beam and scattered light rotated by 90° to the principal axis of the spectrometer; HV, polarization of the incident laser beam at 90° to the principal axis of the spectrometer and the polarization of the scattered light parallel to the principal axis of the spectrometer.

In situ Raman Study of the Deformation of Nanocomposites. For deformation testing, the PMMA beam on which PVA/SWNT electrospun fibers or PVA/SWNT films were deposited was inserted into a four-point bending rig and placed on the Raman microscope stage. The surface strain was measured using a resistance strain gauge. The beam was deformed stepwise and Raman spectra were collected from the nanocomposites at each strain level.

Mechanical Testing of the Films. The mechanical testing was conducted using an Instron-1122 universal testing machine. A vacuum-oven-dried free film was cut into a dumbbell shape with a gage length of 20 mm, a width of 4 mm and the thickness of around 0.12 mm. The samples were left in the mechanical testing room, in which the temperature was set at 23 ± 0.1 °C and the humidity at 50 ± 5%, for at least 48 h prior to mechanical testing. Four samples were tested for each type of film.

ASSOCIATED CONTENT

Supporting Information. S1, orientation of PVA polymers; S2, PVA crystallinity characterized using Raman spectroscopy; S3, effect of dispersion state of nanotubes on Raman band shift rate; S4, angular-dependence of G′-band shift rate for three-dimensional distribution (PDF). This material is available free of charge via the Internet at http://pubs.acs.org.

AUTHOR INFORMATION

Corresponding Author
*Corresponding author: robert.young@manchester.ac.uk.

ACKNOWLEDGMENT

One of the authors (L.D.) is grateful to the Chinese government and UK government for financial support through the "UK-China Scholarship for Excellence" scheme.

REFERENCES

(1) Gupta, S.; Dharamvir, K.; Jindal, V. K. *Phys. Rev. B* **2005,** *72,* 165428 1–16.

(2) Wu, Y.; Huang, M. Y.; Wang, F.; Huang, X. M. H.; Rosenblatt, S.; Huang, L. M.; Yan, H. G.; O'Brien, S. P.; Hone, J.; Heinz, T. F. *Nano Lett.* **2008,** *8,* 4158–4161.

(3) Yu, M. F.; Files, B. S.; Arepalli, S.; Ruoff, R. S. *Phys. Rev. Lett.* **2000,** *84,* 5552–5555.

(4) Yu, M. F.; Lourie, O.; Dyer, M. J.; Moloni, K.; Kelly, T. F.; Ruoff, R. S. *Science* **2000,** *287,* 637–640.

(5) Chou, T.; Gao, L.; Thostenson, E.; Zhang, Z.; Byun, J. *Compos. Sci. Technol.* **2010,** *70,* 1–19.

(6) Chang, C. C.; Hsu, I. K.; Aykol, M.; Hung, W. H.; Chen, C. C.; Cronin, S. B. *ACS Nano* **2010,** *4,* 5095–5100.

(7) Kumar, R.; Cronin, S. B. *J. Nanosci. Nanotechnol.* **2008,** *8,* 122–130.

(8) Sandler, J.; Shaffer, M. S. P.; Windle, A. H.; Morán, M. A. M.; Cooper, C. A.; Young, R. J.; Halsall, M. P. *Phys. Rev. B* **2003,** *67,* 035417 1–8.

(9) Cooper, C. A.; Young, R. J.; Halsall, M. *Compos. Part A* **2001,** *32,* 401–411.

(10) Frogley, M. D.; Zhao, Q.; Wagner, H. D. *Phys. Rev. B* **2002,** *65,* 113413 1–4.

(11) Wood, J. R.; Zhao, Q.; Wagner, H. D. *Compos. Part A* **2001,** *32,* 391–399.

(12) Coleman, J. N.; Khan, U.; Blau, W. J.; Gun'Ko, Y. K. *Carbon* **2006,** *44,* 1624–1652.

(13) Kimura, T.; Ago, H.; Tobita, M.; Ohshima, S.; Kyotani, M.; Yumura, M. *Adv. Mater.* **2002,** *14,* 1380–1383.

(14) Zhang, X.; Liu, T.; Screekumar, T.; Kumar, S.; Hu, X.; Smith, K. *Polymer* **2004,** *45,* 8801–8807.

(15) Dror, Y.; Salahla, W.; Khalfin, R. L.; Cohen, Y.; Yarin, A. L.; Zussman, E. *Langmuir* **2003,** *19,* 7012–7020.

(16) Ji, J.; Sui, G.; Yu, Y.; Liu, Y.; Lin, Y.; Du, Z.; Ryu, S.; Yang, X. *J. Phys. Chem. C* **2009,** *113,* 4779–4785.

(17) Wong, K.; Zinke-Allmanga, M.; Hutter, J. L.; Hrapovi, S.; Luong, J.; Wan, W. *Carbon* **2009,** *47,* 2571–2578.

(18) Kannan, P.; Eichhorn, S. J.; Young, R. J. *Nanotechnology* **2007,** *18,* 235707–235713.

(19) Kannan, P.; Young, R. J.; Eichhorn, S. J. *Small* **2008,** *4,* 930–933.

(20) Dresselhaus, M. S.; Dresselhaus, G.; Saito, R.; Jorio, A. *Phys. Rep.* **2005,** *409,* 47–99.

(21) Hwang, J.; Gommans, H. H.; Ugawa, A.; Tashiro, H.; Haggenmueller, R.; Winey, K. I.; Fischer, J. E.; Tanner, D. B.; Rinzler, A. G. *Phys. Rev. B* **2000,** *62,* R13310–R13313.

(22) Gommans, H. H.; Alldredge, J. W.; Tashiro, H.; Park, J.; Magnuson, J.; Rinzler, A. G. *J. Appl. Phys.* **2000,** *88,* 2509–2514.

(23) Chae, H. G.; Minus, M. L.; Kumar, S. *Polymer* **2006,** *47,* 3494–3504.

(24) Liu, T.; Kumar, S. *Chem. Phys. Lett.* **2003,** *378,* 257–262.

(25) Cronin, S. B.; Swan, A. K.; Ünlü, M. S.; Goldberg, B. B.; Dresselhaus, M. S.; Tinkham, M. *Phys. Rev. B* **2005,** *72,* 035425 1–8.

(26) Deng, L.; Young, R. J.; van der Zwaag, S.; Picken, S. *Polymer* **2010,** *51,* 2033–2039.

(27) Andrews, M. C.; Day, R. J.; Hu, X.; Young, R. J. *J. Mater. Sci. Lett.* **1992,** *11,* 1344–1346.

(28) Buschow, K. H. J.; Cahn, R. W.; Flemings, M. C.; Ilschner, B.; Kramer, E. J.; Mahajan, S. *Encyclopedia of Materials: Science and Technology* **2001,** 2405.

(29) Hull, D. *An Introduction to Composite Materials*; Cambridge University Press: Cambridge, U.K., 1981.

(30) Cronin, S. B.; Swan, A. K.; Unlu, M. S.; Goldberg, B. B.; Dresselhaus, M. S.; Tinkham, M. *Phys. Rev. Lett.* **2004,** *93,* 167401 1–4.

(31) Kumar, R.; Cronin, S. B. *Phys. Rev. B* **2007,** *75,* 155421 1–4.

(32) Young, K.; Blighe, F. M.; Vilatela, J. J.; Windle, A. H.; Kinloch, I. A.; Deng, L.; Young, R. J.; Coleman, J. N. *ACS Nano* **2010,** *4,* 6989–6997.